Evaluation of 3-D bioactive glass scaffolds dissolution in a perfusion flow system with X-ray microtomography

Sheng Yue, Peter D. Lee, Gowsihan Poologasundarampillai, Julian R. Jones *

Department of Materials, Imperial College London, London SW7 2AZ, UK

ABSTRACT

Bioactive glass has high potential for bone regeneration due to its ability to bond to bone and stimulate osteogenesis whilst dissolving in the body. Although three-dimensional (3-D) bioactive glass scaffolds with favorable pore networks can be made from the sol–gel process, compositional and structural evolutions in their porous structures during degradation in vivo, or in vitro, have not been quantified. In this study, bioactive glass scaffolds were put in a simulated body fluid flow environment through a perfusion bioreactor. X-ray microtomography (μCT) was used to non-destructively image the scaffolds at different degradation stages. A new 3-D image processing methodology was developed to quantify the scaffold's pore size, interconnect size and connectivity from μCT images. The accurate measurement of individual interconnect size was made possible by a principal component analysis-based algorithm. During 28 days of dissolution, the modal interconnect size in the scaffold was reduced from 254 to 206 μm due to the deposition of mineral phases. However, the pore size remained unchanged, with a mode of 682 μm. The data presented are important for making bioactive glass scaffolds into clinical products. The technique described for imaging and quantifying scaffold pore structures as a function of degradation time is applicable to most scaffold systems.

© 2011 Acta Materialia Inc. Published by Elsevier Ltd. All rights reserved.

1. Introduction

Synthetic bone grafts (scaffolds) are needed that can regenerate diseased or damaged bone, replacing the need for autografts. Autografts are the current gold standard whereby bone is transplanted, usually from the pelvis. Their disadvantage is the lack of supply and donor site morbidity, which can cause pain and other complications. Scaffolds are also vital components in bone tissue engineering strategies, where the aim is to culture cells on scaffolds prior to implantation. Scaffolds for bone regeneration are designed to act as temporary templates for bone and blood vessel growth. To do this they require a three-dimensional (3-D) porous network [1–3] with high porosity and connectivity for solute transport; with suitable pore and, more importantly, interconnect size distributions to enable cell migration, bone ingrowth and vascularization. The minimum interconnect diameter for human bone ingrowth is generally considered to be 100 μm [4,5]. The scaffold should also form a direct bond to the host bone by enabling cell adhesion and activity. Ideally the scaffold would degrade as the host bone forms, with the degradation products encouraging osteogenesis [2,6]. With all these different criteria to match, a method for quantifying degradation in vitro is needed as a first screening tool for new scaffolds.

Bioactive glasses are promising materials for bone tissue engineering scaffold fabrication [6,7]. They can bond to bone, degrade in the body and release ions which stimulate bone regeneration. When implanted in the body, bioactive glasses form a surface layer of crystalline hydroxyl carbonate apatite (HCA) [8–10], which is similar to bone mineral and is responsible for glass bonding with bone. The osteogenic property of these glasses has been attributed to the release of soluble silica and calcium ions during dissolution [6]. Using a sol–gel foaming process, 3-D bioactive glass scaffolds can be fabricated from bioactive glasses [11], achieving compressive strengths [2,12] and pore structures similar to human trabecular bone, with macropore diameters of 300–600 μm and interconnect diameters in excess of 100 μm [13]. Having achieved structural similarity, quantifying their dissolution behavior is another essential step in their development.

X-ray microtomography (μCT, micro-CT or XMT) can non-destructively image scaffolds in three dimensions [14,15]. Coupled with imaging processing, μCT has become an established tool for scaffold quantification [16–19]. For example, the internal pore structure can be characterized from μCT images, providing quantitative information such as: percentage porosity, pore and interconnect size distributions, network connectivity, pore shape and strut thickness [13,20–22]. The interaction between the scaffold material and its host environment, including bone ingrowth, has also been observed and quantified with μCT, both in vivo and ex vivo [20,22–24]. Furthermore, the non-destructive nature of μCT can

---

* Corresponding author. Tel.: +44 20 75946749; fax: +44 20 75946757.
  E-mail address: julian.r.jones@imperial.ac.uk (J.R. Jones).

enable the evaluation of samples in situ, where experiments such as compression and mineral deposition are performed in vitro, whilst non-invasively scanning the scaffold [25–27]. In addition, the 3-D scaffold images can be used to generate meshes for computational fluid dynamic and mechanical simulations [13,28,29]. Therefore, many aspects of the performance of scaffolds can be evaluated and then improved in a non-invasive and quantifiable manner, reducing product design costs and time.

Current bioactivity and degradation tests for bioceramics usually consist of immersing a sample in a fixed volume of simulated body fluid (SBF), then placing it in an incubator and observing the final extent of HCA formation. However, bioactive glasses, and many other bioceramics, are dynamic materials which undergo dissolution before a HCA layer can deposit on their surface. A test that quantifies this precursor stage is required. For example, a high glass concentration can cause calcite to deposit on the glass surface instead of HCA [30]. The in vivo environment is not a closed environment and saturation of ions is not expected. Therefore, the prescreening process for new scaffolds needs improvement. Perfusion bioreactors are widely used in vitro in tissue engineering applications because perfusion flow can enhance mass transport and introduce shear stress, thereby improving tissue growth [31]. The aim of this work is to use a perfusion bioreactor with a local inhomogeneous flow rate, combined with μCT imaging and image analysis, to study the degradation behavior of bioactive glass foam scaffolds in an SBF flow environment. In order to achieve this, new and improved algorithms were needed with better accuracy and greater automation (using a principal component analysis (PCA)-based approach) than those developed previously for scaffold quantification [13,21]. The hypothesis was that the porous scaffold would undergo dissolution over time, causing the interconnects of the pores to open. Secondary objectives were to determine whether the deposition of the HCA layer could be observed using this technique; whether changes in pore size could be measured; and whether preferential flow within the scaffold would cause heterogeneous dissolution.

2. Materials and methods

2.1. Bioactive glass scaffolds synthesis

Bioactive glass foams of 70S30C composition (70 mol.% SiO$_2$, 30 mol.% CaO) were prepared using a sol–gel foaming method as previously described [11,12]. The sol preparation began with mixing 0.2 N nitric acid with deionized water using a magnetic stirrer, followed by addition of tetraethyl orthosilicate (TEOS) and calcium nitrate (all Sigma–Aldrich) in order. The initial molar ratio of water to TEOS (R ratio) was 12:1. Aliquots of 50 ml of the sol were combined with 3 ml of 5 vol.% hydrofluoric acid (HF, catalyst) and 0.35 ml of Teepol (surfactant, Thames Mead Ltd, London), then foamed using vigorous agitation. As the foamed sol approached the gelation point, it was cast into cylindrical Teflon® moulds, sealed and aged at 60 °C for 72 h. Previous work has shown that Teflon® moulds are non-reactive and facilitate removal, as well as improving the homogeneity of the glass composition [32]. The samples were then dried in air for a total of 94 h at 60, 90 and 130 °C. Finally, the scaffolds were stabilized at 600 °C for 3 h and then sintered at 800 °C for 2 h. The thermal processing was optimized in previous studies, with the drying process designed to prevent cracking and the sintering used to improve compressive strength [12].

2.2. Perfusion bioreactor system

An SBF solution, with ion concentrations similar to those of human extracellular fluid, was prepared following the Kokubo method [33]. Cylindrical bioactive glass scaffolds, 6 mm in diameter and 7 mm high and weighing 0.13 ± 0.2 g, together with a length of non-degradable silica glass fibre, were wrapped with Teflon tape and inserted into a Teflon® ring (termed a scaffold assembly). (Note that the silica glass fibre was added to calibrate the X-ray attenuation in the μCT, enabling the change in density of the scaffold to be monitored). The Teflon® ring containing the sample was then placed into the cylindrical chamber of a perfusion bioreactor (Gradient Container, Minucells Minutissue, Weinheim, Germany [34]), as illustrated in Fig. 1. In order to prevent flow from bypassing the scaffold, the outer diameter (12 mm) of the Teflon® ring matched the inner diameter of the chamber, while the Teflon® ring was also wrapped with Teflon® tape to ensure a tight seal. Three samples were run in separate experiments on separate occasions using fresh SBF, but using the same perfusion chamber.

The SBF flow circulation, which was directed through the scaffold from bottom to top with a flow rate of 1 ml min^{-1}, was maintained with a peristaltic pump (Masterflex, model 07519–25, Cole-Palmer Instrument Co., Niles, IL, USA). A 1 l reservoir of SBF was maintained at 37 °C in an incubator.

2.3. Optical emission inductive coupled plasma spectroscopy

For each of the three samples, at dissolution time points of 0, 1, 8, 24 h, 7 days and 28 days, 50 ml of the SBF solution was collected for analysis. The entire SBF was replaced after 7 days. The ion concentrations of P, Si and Ca in the collected solutions were measured with optical emission inductive coupled plasma (ICP) spectroscopy (Thermo Scientific ICP Spectrometer, Model iCAP 6300 Series Duo).

2.4. X-ray microtomography

μCT was used to scan the scaffold assembly as a function of degradation time in SBF flow. Each scaffold assembly was scanned before the dissolution study using a lab-based μCT unit (Phoenix X-ray Systems and Services GmbH, Wunstorf, Germany) at 100 kV and 100 μA, and with a voxel size of 8 μm. At 24 h, 7 days and 28 days, the dissolution experiment was paused and the scaffold assembly was removed out from the bioreactor, dried at 37 °C overnight and rescanned by μCT with the same setting as that of the 0 h scan. After μCT scanning, the assembly was reinstalled and the dissolution experiment resumed.
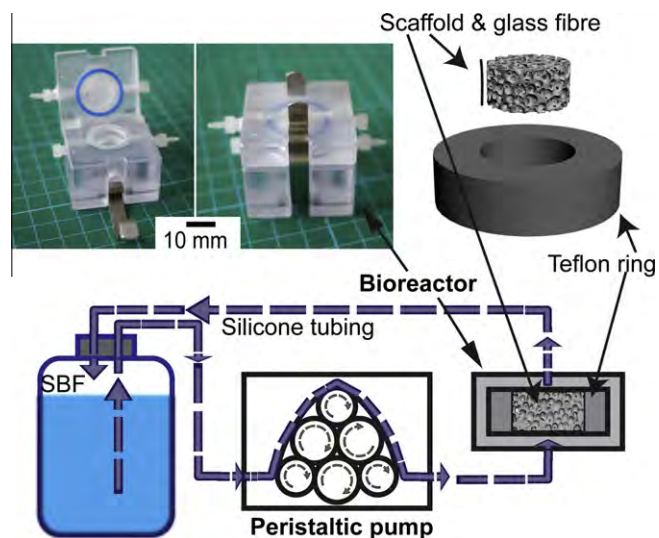
Fig. 1. Schematic of the dissolution experimental setup. The arrows on the silicone tubing indicate the SBF flow direction.

2.5. Scanning electron microscopy and energy-dispersive X-ray spectrometry

Two additional bioactive glass scaffolds were used for electron microscopic analysis as it is destructive – one was scanned a 0 h and the other was immersed in SBF flow for 3 days and then scanned, and one of the three repeats was also scanned after 28 days. Each was dried and scanned using a scanning electron microscope (Leo 1525) equipped for energy-dispersive X-ray spectrometry (EDX) to characterize the morphology as well as the composition. For the 28 days sample, a μCT scan was performed prior to scanning electron microscopy (SEM) and EDX analysis to provide confirmation of the μCT data interpretation.

2.6. Three-dimensional image analysis

The initial stage of 3-D image processing builds on a previously published technique [13,21]. The segmentation process steps are as follows.

1. A $3 \times 3 \times 3$ median filter was applied to all μCT images to remove noise.
2. For each scaffold assembly, the μCT images at 24 h, 7 days and 28 days were numerically registered to the appropriate image taken at 0 h. The registration process resampled the images first (by an initial factor of 4 and a refined factor of 2), then transformed the moving image rigidly (Rigid3-D transform, only rotation and translation), based on the Mean Squares similarity metrics using ITK [35] (Insight Segmentation and Registration Toolkit, ITK).
3. The Teflon® ring and non-degradable silica glass fibre in the μCT images were thresholded and then located using a connected component labeling algorithm [36]. The X-ray attenuation properties of the Teflon® and silica glass fibre were assumed to remain constant, allowing all the μCT images to be normalized to each other.
4. Global thresholding was applied to the normalized images to classify each voxel as either scaffold or background according to its intensity. The thresholding values were determined from histograms of the images, picking the value equidistant for the peak background and scaffold levels.
5. A dilation-based distance transform was then applied to the binarized images. The background phase in the images was filled step by step by dilating of the strut phase (26-connectivity kernel) until all the voxels were filled. The number of steps required to reach each replaced voxel was then recorded as the value of that position, forming a 3-D distance map.
6. Using the pore centroid locations (local maxima in the distance map), a 3-D watershed transform [37] was then applied to the distance map and the background voxels were segmented and labeled as separated macropores according to the topological variation.
7. Any background voxels that neighbored (with 26-connectivity) more than one labeled pore were identified and grouped as interconnects.

Once the background phase in the μCT image was segmented and labeled as macropores and interconnects, the following quantification procedures were applied:

1. The pores and interconnects touching the border of the region of interest were not used for property measurement because they may only be part of the pore/interconnect and the following measuring method would not be appropriate to reflect the sizes of those partial pores/interconnects.

2. The volume, equivalent diameter (the diameter of a sphere with the same volume as a pore), connectivity and many other characteristics of the pores were quantified.

To quantify the interconnect size and morphology, an improved method was developed and applied that was significantly different from previous studies [13,21] (see Fig. 2). This new methodology first located the principal plane of each interconnect (disc shape in Fig. 2c) by a PCA method. The steps used to find the principal plane and then measure the interconnect size are:

1. For each interconnect, the PCA was started by calculating the covariance matrix of its voxels coordinates.
2. The eigenvector which corresponded to the smallest eigenvalue of the covariance matrix is the normal to the interconnect's principal plane. The principal plane also passes the centroid of the interconnect voxels. Therefore, for each interconnect in the 3-D space, there is only one unique principal plane, which can be located by its normal and the centroid of the interconnect.
3. In order to measure the interconnect size, all voxels of a given interconnect were projected to its principal plane. This allows the 3-D disc-like shape to be reduced to a 2-D projection. A convex hull algorithm was then used to determine the effective
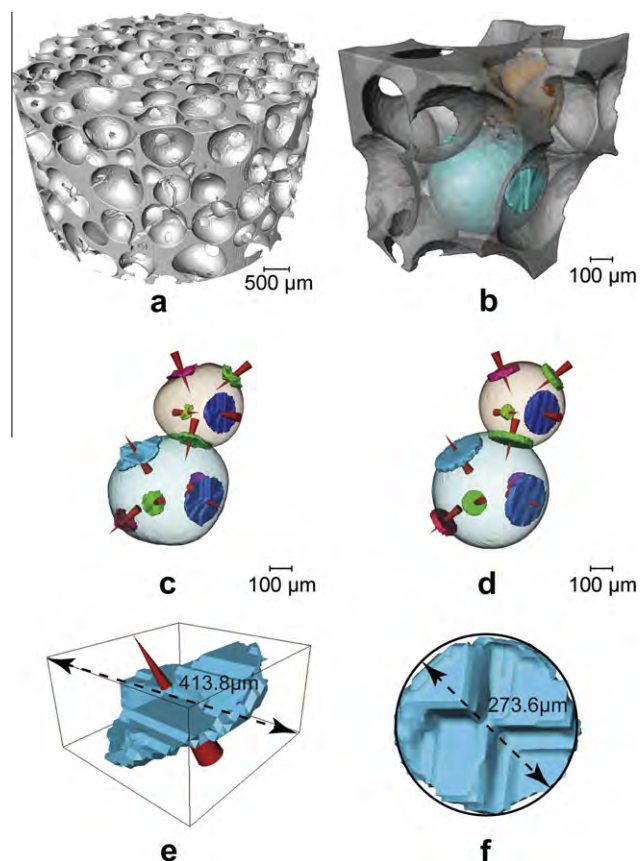
Fig. 2. 3-D rendering of μCT images show: (a) a 3-D porous bioactive glass foam scaffold; (b) a sub-volume of the scaffold containing two color-labeled pores (scaffold struts rendered with 50% transparency); (c) two pores from (b) with their neighboring interconnects; (d) equivalent pores and interconnects of (c) from the quantification algorithms; (e) a single interconnect with its coordinate bounding box. The bounding box diagonal that was used as an equivalent diameter by Atwood et al. [21] was 413.8 μm in length; (f) the same interconnect in (e) which was rotated to its principal plane. The length of the equivalent diameter, which was obtained by the PCA method, was 273.6 μm. In (c) and (d), pores were rendered with 50% transparency, and each cone indicates the normal of the principal plane for every interconnect.

area of the interconnect's projection in two dimensions. An equivalent diameter was also determined equal to the diameter of a circle with the same area as the interconnect.
4. The distributions of the pore size and interconnect size for each scaffold were produced, weighted by volume fraction and equivalent area fraction, respectively.

This new method of performing a PCA of the interconnects and then measuring them in the principal plane significantly improved the accuracy of the dimensions obtained, as shown by comparing Fig. 2e and f. In this example the bounding box diagonal of the single interconnect was 414 μm (using the method from Ref. [21]), where the equivalent diameter of the same interconnect obtained by the PCA method was 274 μm, showing a 51% improvement over the old method.

3. Results

High-resolution μCT allowed the non-destructive scanning of the same bioactive glass scaffold at a series of dissolution time points and, by registering these scans with respect to each other, a highly accurate quantification of the dissolution kinetics was determined. The changes in one scaffold at four dissolution time points is shown in Fig. 3a–d as a 3-D rendering and as 2-D slices in Fig. 3e–h (perpendicular to the flow direction). The regions with higher intensity values in the volume image indicate where the material has a higher X-ray attenuation, and are rendered with a warmer color in Fig. 3. The scaffold phase had a higher intensity level than the background phase, which was easily distinguished. The amount of attenuation was a combination of both the composition (higher atomic number atoms attenuate more) and density; correlations between the μCT scan and SEM-EDX illustrated that the red regions contained a greater percentage of calcium. Fig. 3a and e shows the initial pore network prior to dissolution (0 h). The color variation of the struts reflects the inhomogeneous initial composition within the amorphous scaffold; note that the high X-ray attenuating material was observed more frequently close to the surface of the struts.

After 24 h in SBF flow, there was a slight reduction in overall image intensity level (compare Fig. 3b and f to a and e). However, the reduction was quite heterogeneous: the voxel intensity reduced much more in some regions than in others, whilst in some regions the intensity increased. These observations suggest that in SBF flow conditions material leached out from the struts of the scaffold unevenly, while redepositing at other locations.

After 7 days of immersion (Fig. 3c and g), the voxel intensity level of the volume image significantly reduced compared to the 0 and 24 h images, indicating dissolution of calcium. In addition, there was a significant decrease in the size of many interconnects, with only a few increasing in size. After 7 days there were also a number of regions of localized deposition of highly attenuating species at the periphery of a number of pores in the top left-hand corner of the scaffold (red and yellow regions), which were not present at 0 and 24 h. As confirmed below using EDX, these were depositions of Ca-rich mineral phases. After 28 days of immersion (Fig. 3d and f), almost all areas of the scaffold showed reduced attenuation. The exceptions were the upper left region in the 3-D image and the top and bottom regions in the 2-D slice, which had highly attenuating (red) regions in the walls and around the periphery of many of the pores. The deposition of Ca-rich phases that began at 7 days seemed to have increased at 28 days, shown by an increase in red intensity at the pore surface in Fig. 3d compared to Fig. 3c.

The quantification illustrates that all pores were well connected, with a mean of five disc-like interconnects to neighboring
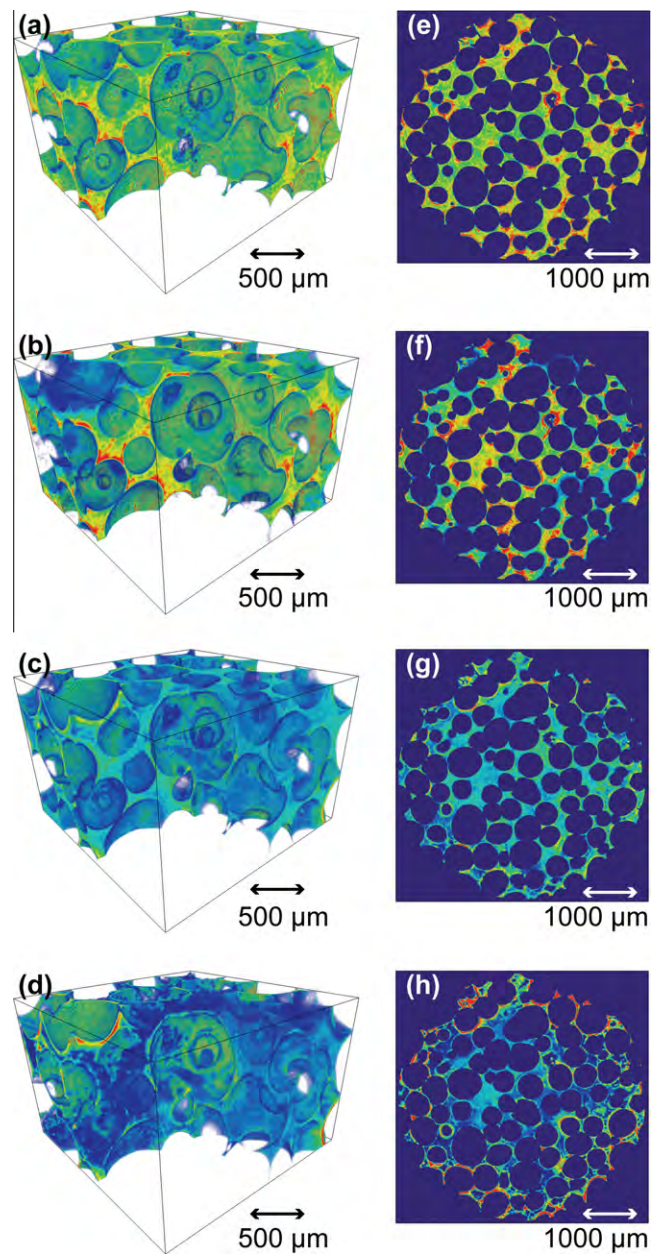
Fig. 3. 3-D sub-volumes and transverse slices (perpendicular to the flow direction) from the normalized μCT images of the scaffold at time points of 0 h (a, e), 24 h (b, f), 7 days (c, g) and 28 days (d, h). (Note, the colors indicate relative X-ray attenuation and are all normalized to each other. Warmer color indicates higher attenuation material).

pores, 3.6 (72%) of which, on average, had an equivalent diameter greater than 100 μm (Fig. 4b). The modal equivalent pore diameter remained unchanged at 682 μm for the four time points; however, there was a slight broadening of the pore size distribution at 28 days towards smaller pores, as deposition on the insides of the pores occurs. Prior to dissolution, 95% (in area) of interconnects had an equivalent diameter larger than 100 μm, with a modal value of 254 μm. After 24 h, the distribution became skewed to slightly smaller interconnect sizes (modal value of 254 μm), which had reduced further to 206 μm after 7 days. The reduction in average interconnect size halted after 7 days, with the mode remaining at 206 μm at 28 days. Note that although the average reduced, there were locations where the interconnect size enlarged, but this was less common. Note also that throughout the dissolution
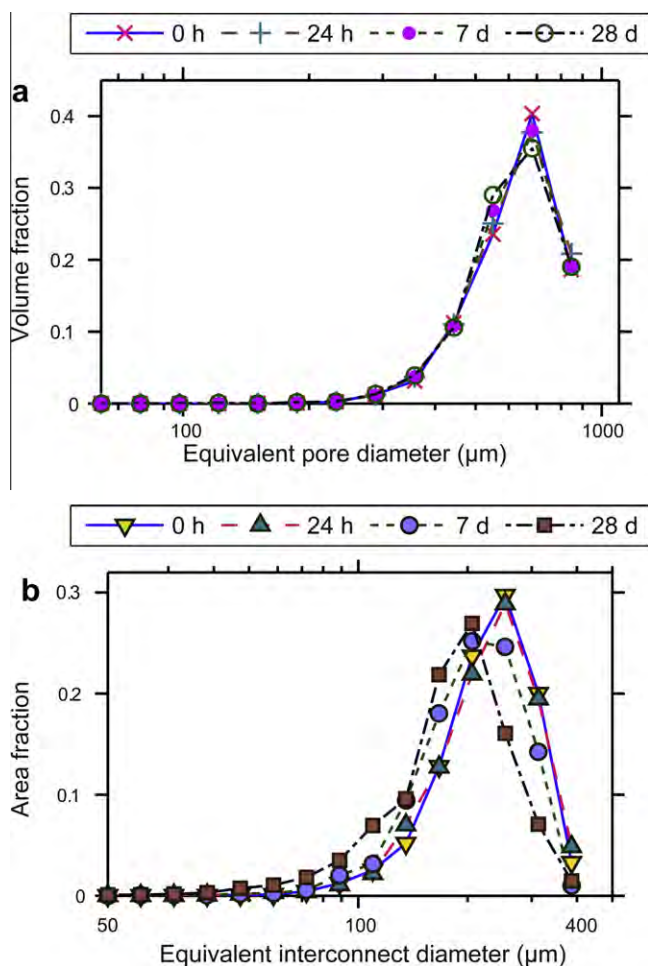
Fig. 4. Size distributions of the equivalent diameter of the (a) pores and (b) interconnects.

process 95% of the interconnects remained larger than 100 μm, providing an easy transport mechanism of nutrients and cells between macropores.

The 0 h struts had a uniform surface (Fig. 5a) and the EDX analysis (Fig. 5d) gave a composition similar to the nominal composition of the bioactive glass, i.e. 70 mol.% of SiO₂ and 30 mol.% of CaO. After 3 days in SBF flow the scaffold's surface had become roughened in some regions (Fig. 5b), perhaps due to partial dissolution. EDX (Fig. 5e) of these regions showed a significant reduction in Ca, supporting the calcium dissolution hypothesis. After 28 days (Fig. 5c), a material with a crystalline appearance covered most scaffold surface areas. EDX analysis (Fig. 5f) of this deposit indicated high calcium and phosphorous levels, suggesting that an HCA layer had formed. The presence of this crystalline structure was observed on all the scaffold surfaces imaged in the scanning electron microscope for the 28 days sample.

Changes in the SBF Si, P and Ca levels with time relative to the initial composition are plotted in Fig. 6, as determined by ICP analysis. During the first 7 days, the Si level increased by 8.8 ppm (Fig. 6a). The P levels decreased after 7 days, probably due to phosphate depositing on the glass surface as calcium phosphate-rich phases (Fig. 6b) [26]. Ca levels increased slightly in the first 24 h (Fig. 6c), due to an initial burst of Ca dissolution, exceeding the rate of redeposition. After 7 days, the Ca level decreased to 5.7 ppm lower than fresh SBF after 7 days, indicating that the deposition of Ca-rich phases dominates over dissolution. After sampling at 7 days, the SBF solution was completely replaced with fresh med-

ium. Over the next 21 days, the Ca and P levels dropped considerably, indicating further deposition of calcium phosphate-rich phases (as confirmed via EDX above and the decrease in pore size in Fig. 4a).

4. Discussion

The non-destructive and non-invasive nature of μCT enabled the capture of the changing structure of bioactive glass scaffolds during dissolution for the first time. Quantification of the μCT scans of the sol–gel-derived 70S30C bioactive glass foam showed that throughout 28 days of degradation it retained its interconnected porous network suitable for bone regeneration applications both in terms of pore size and interconnect diameter. The pore size had a log-normal distribution, with a mode of 682 μm, which did not change over 28 days of immersion. The macropores within the network were well connected (with an average of 3.6 large interconnects per pore). More importantly, the majority of interconnects (95% of their total area) had equivalent diameters in excess of 100 μm, meaning that they are potentially large enough for vascularized bone growth throughout the scaffold.

When characterizing the porous structure of a scaffold, a transition from qualitative interpretation to quantitative measurement was made possible with the novel 3-D image analysis techniques. The 3-D scan of the scaffold was segmented using a sequence of image processing algorithms as described in Materials and methods above. The measurement of the interconnect sizes has been made more accurate compared to previous work (51% for the example given in the Methods Section), and fully automated by introducing a PCA-based algorithm. The PCA algorithm allows objects that are randomly oriented in 3-D space to be aligned such that an optimal projection onto a 2-D plane is achieved and a more accurate measurement obtained. Although this method was demonstrated using interconnects in this study, the methodology is applicable to a wide range of features, from bone nodules to fibrous features in composite scaffolds. The improvement obtained by this method is limited to objects that are elongated in either one or two directions (i.e. that have one or two strong principal components).

The μCT quantification showed that calcium distribution in the unreacted scaffolds was not homogeneous. The sol–gel process was previously thought to be a method of choice for producing homogeneous compositions. However, previous work has shown that the use of calcium nitrate as a calcium precursor, which is the traditional choice, does not give a homogeneous calcium distribution [32]. Here, the μCT showed this to be true in foams. The inhomogeneity was due to the calcium nitrate being soluble in water and calcium not going into the silica network until a temperature of 400 °C was reached. After drying, the struts consist of silica nanoparticles coated with calcium nitrate. During stabilization and sintering, the nanoparticles fused together, the calcium nitrate dissociated and calcium diffused into the struts. The foams have greater homogeneity than monoliths [32] but cannot be considered to be completely homogeneous.

During dissolution there were two dominant events: dissolution of the scaffold followed by mineral deposition. Over the first 24 h, calcium content was depleted near the surface of the scaffold due to exchange of calcium ions with H⁺ from the solution. Soluble silica was also lost to the solution. μCT quantification showed that the majority of interconnects shrunk slightly during the first 7 days period, but the pore size remained similar. The interconnects shrunk as calcium phosphate was deposited on the surface of the scaffolds, growing into the interconnect region. This was confirmed both by ICP, where a reduction of Ca and P was measured in SBF, and via SEM–EDX, where deposits were visually observed and Ca and P were quantified by EDX. In addition, μCT showed a decrease
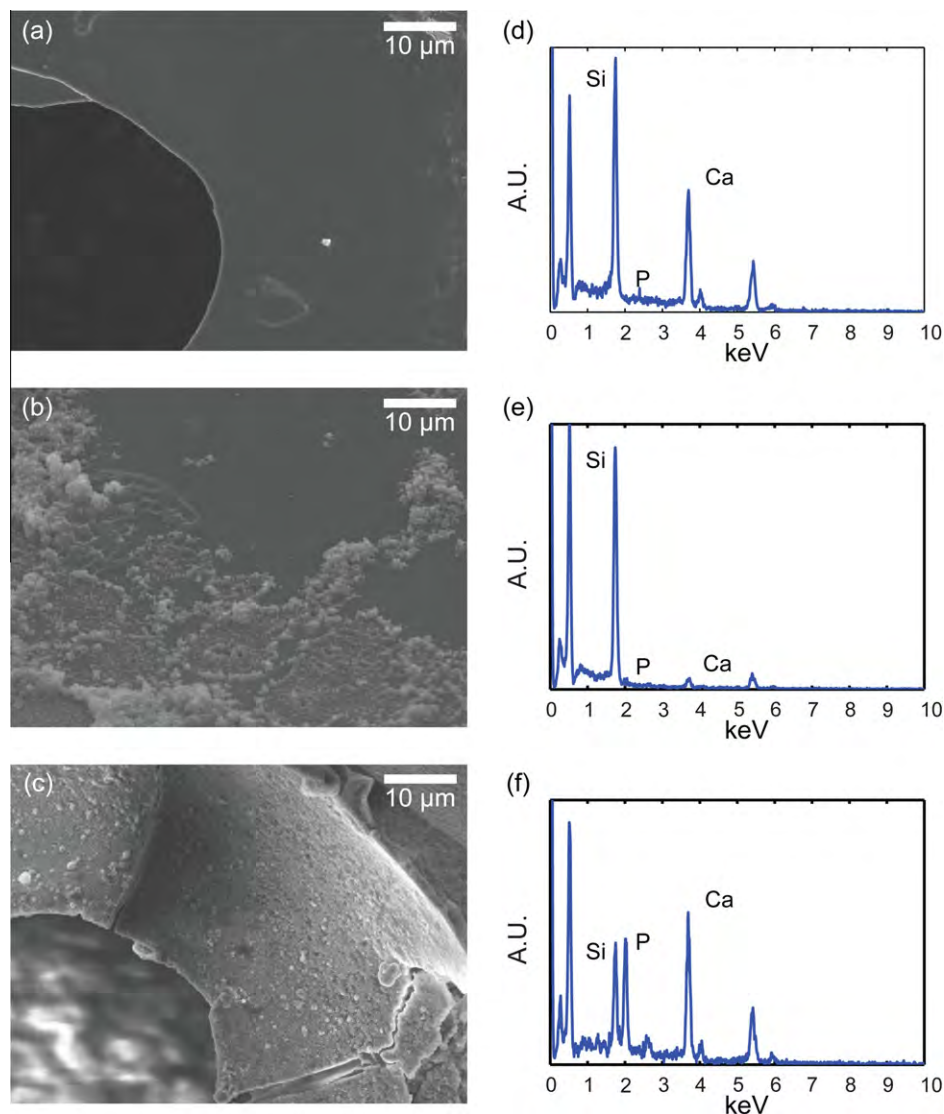
Fig. 5. SEM images (a–c) and associated EDX (d–f) analysis of the 70S30C bioactive scaffolds at 0 h (a, d), 3 days (b, e) and 28 days (c, f) time points.

in calcium (shown by X-ray attenuation) within the scaffold and an increase in dense/high atomic number deposits on the pore surfaces, including near the interconnects. Note that a few interconnects enlarged, indicating preferential flow channels formed in the perfusion bioreactor, causing dissolution of the glass at edges of these interconnects. Unfortunately, since a laboratory source μCT machine was used with polychromatic X-rays, only the relative changes in calcium level, rather than the absolute levels, could be determined.

The 3-D μCT images and image analysis indicated that there was little change in the strut morphology between 7 and 28 days, which implies that the silica did not continue to degrade. The ICP results agree with this, as the silica content of the SBF increased less between 7 and 10 days than between 0 and 7 days. The local pH must be greater than nine for Si—O—Si bonds to break and for soluble silica to be released, and this is quite likely in flow conditions in the first 7 days as the calcium was released by the glass. The flow then removed the calcium ions from close to the glass, causing a buffering effect. The HCA deposition will also reduce the surface area of the glass that is in contact with the SBF. Bioactive glasses have been found to degrade in vivo; therefore long-term degradation must be due to the action of osteoclasts. This is

preferable to continual degradation by aqueous dissolution as degradation by continuous dissolution may be too fast to allow bone remodelling to occur, which can take weeks or months, depending on the defect site.

5. Conclusions

High-resolution μCT was used for the first time to non-destructively image 3-D sol–gel-derived bioactive glass scaffolds during the dissolution process in SBF flow. The 3-D image analysis techniques required significant improvement from previous work to provide accurate quantification. This was done by introducing a PCA-based method to fully automatically measure the interconnect sizes within the scaffold, providing an increased accuracy. The quantification shows that the sol–gel-derived 70S30C bioactive glass foam has a suitable porous structure for use as a bone tissue engineering scaffold. The pore size remained relatively unchanged, with a constant mode of 682 μm, whereas the interconnects reduced slightly in size (from 254 to 206 μm) due to the deposition of mineral phases. A crystalline phase matching the composition of hydroxyl carbonate apatite was found to form over the majority of the scaffold after 28 days in an SBF flow environment.
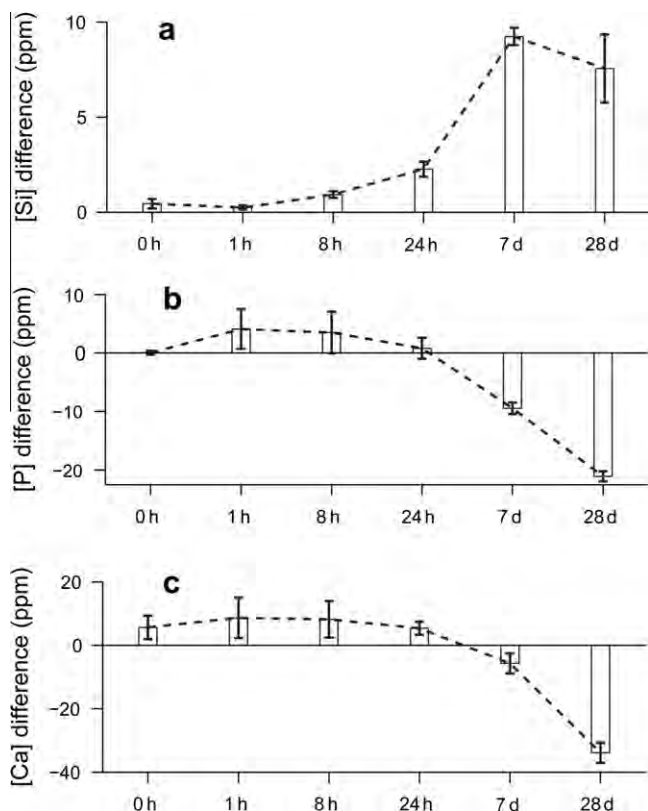
Fig. 6. ICP analysis for the (a) Si, (b) P and (c) Ca ion concentrations in SBF solution at each time point.

Acknowledgements

References

[1] Langer R, Vacanti JP. Tissue engineering. Science 1993;260:920–6.
[2] Jones JR, Lee PD, Hench LL. Hierarchical porous materials for tissue engineering. Phil Trans R Soc A 2006;364:263–81.
[3] Emadi R, Tavangarian F, Esfahani SIR, Sheikhhosseini A, Kharaziha M. Nanostructured forsterite coating strengthens porous hydroxyapatite for bone tissue engineering. J Am Ceram Soc 2010;93:2679–83.
[4] Hulbert SF, Morrison SJ, Klawitter JJ. Tissue reaction to three ceramics of porous and non-porous structures. J Biomed Mater Res 1972;6:347–74.
[5] Gauthier O, Bouler J-M, Aguado E, Pilet P, Daculsi G. Macroporous biphasic calcium phosphate ceramics: influence of macropore diameter and macroporosity percentage on bone ingrowth. Biomaterials 1998;19:133–9.
[6] Hench LL, Polak JM. Third-generation biomedical materials. Science 2002;295:1014–7.
[7] Xynos ID, Edgar AJ, Buttery LDK, Hench LL, Polak JM. Gene-expression profiling of human osteoblasts following treatment with the ionic products of Bioglass® 45 S 5 dissolution. J Biomed Mater Res 2001;55:151–7.
[8] Hench LL, Paschall HA. Direct chemical bond of bioactive glass–ceramic materials to bone and muscle. J Biomed Mater Res 1973;7:25–42.
[9] Kokubo T, Takadama H. How useful is SBF in predicting in vivo bone bioactivity? Biomaterials 2006;27:2907–15.
[10] Emadi R, Tavangarian F, Esfahani SIR. Biodegradable and bioactive properties of a novel bone scaffold coated with nanocrystalline bioactive glass for bone tissue engineering. Mater Lett 2010;64:1528–31.
[11] Sepulveda P, Jones JR, Hench LL. Bioactive sol–gel foams for tissue repair. J Biomed Mater Res 2002;59:340–8.
[12] Jones JR, Ehrenfried LM, Hench LL. Optimising bioactive glass scaffolds for bone tissue engineering. Biomaterials 2006;27:964–73.
[13] Jones JR, Poologasundarampillai G, Atwood RC, Bernard D, Lee PD. Non-destructive quantitative 3D analysis for the optimisation of tissue scaffolds. Biomaterials 2007;28:1404–13.
[14] Stock SR. X-ray microtomography of materials. Int Mater Rev 1999;44:141–64.
[15] Stock SR. Recent advances in X-ray microtomography applied to materials. Int Mater Rev 2008;53:129–81.
[16] van Lenthe GH, Hagenmuller H, Bohner M, Hollister SJ, Meinel L, Müller R. Nondestructive micro-computed tomography for biological imaging and quantification of scaffold-bone interaction in vivo. Biomaterials 2007;28:2479–90.
[17] Guldberg RE, Duvall CL, Peister A, Oest ME, Lin ASP, Palmer AW, et al. 3D imaging of tissue integration with porous biomaterials. Biomaterials 2008;29:3757–61.
[18] Jones JR, Atwood RC, Poologasundarampillai G, Yue S, Lee PD. Quantifying the 3D macrostructure of tissue scaffolds. J Mater Sci Mater Med 2009;20:463–71.
[19] Renghini C, Komlev V, Fiori F, Verné E, Baino F, Vitale-Brovarone C. Micro-CT studies on 3-D bioactive glass-ceramic scaffolds for bone regeneration. Acta Biomater 2009;5:1328–37.
[20] Bohner M, Van Lenthe GH, Grünenfelder S, Hirsiger W, Evison R, Müller R. Synthesis and characterization of porous [beta]-tricalcium phosphate blocks. Biomaterials 2005;26:6099–105.
[21] Atwood RC, Jones JR, Lee PD, Hench LL. Analysis of pore interconnectivity in bioactive glass foams using X-ray microtomography. Scripta Mater 2004;51:1029–33.
[22] Jones AC, Arns CH, Hutmacher DW, Milthorpe BK, Sheppard AP, Knackstedt MA. The correlation of pore morphology, interconnectivity and physical properties of 3D ceramic scaffolds with bone ingrowth. Biomaterials 2009;30:1440–51.
[23] Cartmell S, Huynh K, Lin A, Nagaraja S, Guldberg R. Quantitative microcomputed tomography analysis of mineralization within three-dimensional scaffolds in vitro. J Biomed Mater Res A 2004;69A:97–104.
[24] Jones AC, Arns CH, Sheppard AP, Hutmacher DW, Milthorpe BK, Knackstedt MA. Assessment of bone ingrowth into porous biomaterials using MICRO-CT. Biomaterials 2007;28:2491–504.
[25] Ohgaki T, Toda H, Kobayashi M, Uesugi K, Kobayashi T, Niinomi M, et al. In-situ high-resolution X-ray CT observation of compressive and damage behaviour of aluminium foams by local tomography technique. Adv Eng Mater 2006;8:473–5.
[26] Yue S, Lee PD, Poologasundarampillai G, Yao Z, Rockett P, Devlin A, et al. Synchrotron X-ray microtomography for assessment of bone tissue scaffolds. J Mater Sci Mater Med 2010;21:847–53.
[27] Hagenmüller H, Hofmann S, Kohler T, Merkle H, Kaplan D, Vunjak-Novakovic G, et al. Non-invasive time-lapsed monitoring and quantification of engineered bone-like tissue. Ann Biomed Eng 2007;35:1657–67.
[28] Porter B, Zauel R, Stockman H, Guldberg R, Fyhrie D. 3-D Computational modeling of media flow through scaffolds in a perfusion bioreactor. J Biomech 2005;38:543–9.
[29] Singh R, Lee PD, Lindley TC, Dashwood RJ, Ferrie E, Imwinkelried T. Characterization of the structure and permeability of titanium foams for spinal fusion devices. Acta Biomater 2009;5:477–87.
[30] Jones JR, Sepulveda P, Hench LL. Dose-dependent behavior of bioactive glass dissolution. J Biomed Mater Res 2001;58:720–6.
[31] Porter BD, Lin ASP, Peister A, Hutmacher D, Guldberg RE. Noninvasive image analysis of 3D construct mineralization in a perfusion bioreactor. Biomaterials 2007;28:2525–33.
[32] Lin S, Ionescu C, Baker S, Smith ME, Jones JR. Characterisation of the inhomogeneity of sol–gel-derived SiO₂–CaO bioactive glass and a strategy for its improvement. J Sol–Gel Sci Technol 2010;53:255–62.
[33] Kokubo T. Bioactive glass ceramics: properties and applications. Biomaterials 1991;12:155–63.
[34] Seitz S, Ern K, Lamper G, Docheva D, Drosse I, Milz S, et al. Influence of in vitro cultivation on the integration of cell–matrix constructs after subcutaneous implantation. Tissue Eng 2007;13:1059–67.
[35] Ibáñez L, Schroeder W, Ng L, Cates J, Consortium IS. The ITK Software Guide. Second edition, updated for ITK version 2.4, 2005.
[36] Haralick R, Shapiro L. Computer and robot vision. Boston, MA: Addison-Wesley Longman Publishing Co.; 1992.
[37] Mangan AP, Whitaker RT. Partitioning 3-D surface meshes using watershed segmentation. IEEE Trans Visual Comput Graphics 1999;5:308–21.